Journal of Zhejiang University-SCIENCE A (Applied Physics & Engineering)
ISSN 1673-565X (Print); ISSN 1862-1775 (Online)
www.zju.edu.cn/jzus; www.springerlink.com
E-mail: jzus@zju.edu.cn

Recursive calibration for a lithium iron phosphate battery for electric vehicles using extended Kalman filtering*

Xiao-song HU†, Feng-chun SUN, Xi-ming CHENG†‡

(*National Engineering Laboratory for Electric Vehicles, Department of Mechanical Engineering, Beijing Institute of Technology, Beijing 100081, China*)

†E-mail: huxstank@bit.edu.cn; cxm2004@bit.edu.cn

Received May 20, 2011; Revision accepted Sept. 8, 2011; Crosschecked Sept. 29, 2011

Abstract: In this paper, an efficient model structure composed of a second-order resistance-capacitance network and a simply analytical open circuit voltage versus state of charge (SOC) map is applied to characterize the voltage behavior of a lithium iron phosphate battery for electric vehicles (EVs). As a result, the overpotentials of the battery can be depicted using a second-order circuit network and the model parameterization can be realized under any battery loading profile, without a special characterization experiment. In order to ensure good robustness, extended Kalman filtering is adopted to recursively implement the calibration process. The linearization involved in the calibration algorithm is realized through recurrent derivatives in a recursive form. Validation results show that the recursively calibrated battery model can accurately delineate the battery voltage behavior under two different transient power operating conditions. A comparison with a first-order model indicates that the recursively calibrated second-order model has a comparable accuracy in a major part of the battery SOC range and a better performance when the SOC is relatively low.

Key words: Model calibration, Lithium iron phosphate battery, Electric vehicle (EV), Extended Kalman filtering
doi:10.1631/jzus.A1100141 **Document code:** A **CLC number:** TM912.1

1 Introduction

Electric vehicles (EVs) are playing an increasingly important role in reducing fuel consumption and lowering poisonous emissions in ground transportation (Sciarretta *et al*., 2004; Lin *et al*., 2008; Xiong *et al*., 2009). Traction battery packs, important components of EVs, directly determine the performance of EVs in actual daily driving. In order to pursue an optimal efficiency of energy utilization, a good battery management system is required to monitor battery internal states that cannot be directly measured in actual operations of EVs, such as state of charge (SOC) and state of health (SOH) (Hu *et al*., 2010a; 2010b; Sun *et al*., 2011). In order to effectively indicate these unmeasured states, a battery model that can essentially describe the battery dynamical behavior is needed.

For on-board battery management applications for EVs, a good battery model should be sufficiently accurate, adaptable and have a moderate structure. An electrochemical battery model often can depict the battery voltage response very accurately. However, this type of model, including a set of partial differential equations, is too complicated to guarantee a high computational efficiency, which is required for actual on-board applications. To seek a compromise between model accuracy and complexity, equivalent circuit-based and simplified electrochemistry-based model structures have often been investigated. Open circuit voltages (OCVs) in many equivalent circuit-based models have often been represented by the tabulated OCV-SOC data determined beforehand (Lin *et al*., 2005; Kim, 2006; 2008; Li, 2007; Qiang *et al*.,

‡ Corresponding author
* Project (No. 61004092) supported by the National Natural Science Foundation of China

2008; Dai *et al*., 2009). The accuracy of this type of model is thus strongly dependent on the reliability of the tabulated data. Nevertheless, the experiments for specially collecting the tabulated OCV-SOC data are often time-consuming and error-prone, especially for lithium iron phosphate batteries, which have quite flat OCV-SOC curves. Although many simplified electrochemical battery models featured an analytical OCV-SOC map which can make experiments for ascertaining OCV values unnecessary (Plett, 2004; Wang *et al*., 2007; Han *et al*., 2009; Sun *et al*., 2011), their ability to describe the battery polarization voltage was often limited.

On the other hand, most versions of the two types of battery models have been parameterized using batch methods, sometimes yielding poor robustness against varying battery operations. Thus, the recursive least squares algorithm with forgetting factors has been used to online calibrate first-order battery models (Verbrugge, 2007; Hu *et al*., 2011). However, in many cases, the standard least squares-based identification methods are only applicable for linear battery model identification. If a linear identifiable form of the battery model is very difficult or impossible to be derived, the classic linear-system-identification approaches might be nonfeasible. Therefore, the advanced extended Kalman filtering has been proposed to recursively identify nonlinear battery models (Plett, 2004). Nevertheless, the structure of the "enhanced self-correcting" model was so complicated that tuning the extended Kalman filter was a very difficult task and a good computational efficiency was challenging to be attained. Extended Kalman filtering has also been used to calibrate the internal resistance of a lithium ion battery (Dai *et al*., 2009). However, recursively identifying the internal resistance did not completely characterize the battery behavior online from the viewpoint of system identification.

In this paper, an efficient model structure is applied to depict the voltage behavior of an EV lithium iron phosphate battery. The model structure consists of a second-order resistance-capacitance network and a simply analytical representation of OCV-SOC map so that the advantages of both the second-order circuit network and simplified electrochemistry-based models can be effectively combined. To pursue a good adaptability, extended Kalman filtering is used to recursively calibrate the second-order model. The linearization associated with extended Kalman filtering is realized through recurrent derivatives in a recursive fashion. A comparison with a first-order model with the same OCV structure is also made.

2 Battery model structure

The battery model structure is shown in Fig. 1. V_{oc} denotes OCV, which is depicted by the Nernst equation with respect to the battery SOC S. K_0 and K_1 are two unknown parameters (Ota *et al*., 2008). Two resistance-capacitance networks are used to simulate the overpotential effects of the battery: the R_1C_1 network is used for the fast time-constant behavior of the battery and the R_2C_2 network for the relatively slow time-constant behavior. R_3 is the ohmic resistance, V_t is the output voltage of the model, and I is the current.

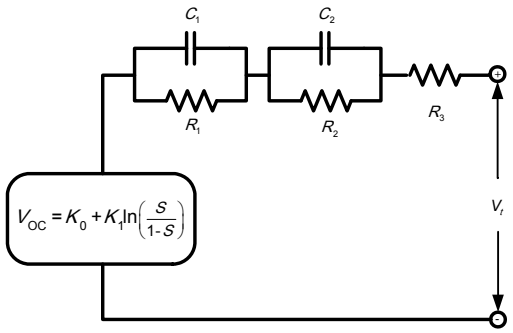

Fig. 1 Battery model structure

According to basic principles of the electrical circuits, the discrete-time state equations can be described as follows:

$$\begin{bmatrix} S_{k+1} \\ V_{1,k+1} \\ V_{2,k+1} \end{bmatrix} = \begin{bmatrix} 1 & 0 & 0 \\ 0 & \alpha_1 & 0 \\ 0 & 0 & \alpha_2 \end{bmatrix} \begin{bmatrix} S_k \\ V_{1,k} \\ V_{2,k} \end{bmatrix} + \begin{bmatrix} -\eta \Delta t / C_n \\ b_1 \\ b_2 \end{bmatrix} I_k, \quad (1)$$

where

$$\alpha_1 = e^{\frac{-\Delta t}{R_1 C_1}}, \quad (2)$$

$$\alpha_2 = e^{\frac{-\Delta t}{R_2 C_2}}, \quad (3)$$

$$b_1 = R_1 - R_1 e^{\frac{-\Delta t}{R_1 C_1}}, \quad (4)$$

$$b_2 = R_2 - R_2 \mathrm{e}^{\frac{-\Delta t}{R_2 C_2}}, \tag{5}$$

where V_1 and V_2 represent the voltages across C_1 and C_2, respectively; η is the Coulombic efficiency; C_n is the nominal capacity; Δt is the sampling time; and the subscript k is the time step index. The output equation of the model is described by

$$V_{t,k} = K_0 + K_1 \ln\left(\frac{S_k}{1-S_k}\right) - V_{1,k} - V_{2,k} - I_k R_3. \tag{6}$$

3 Battery calibration algorithm based on extended Kalman filtering

In order to apply extended Kalman filtering to identify the model parameters, the calibration process of the battery should be represented in a state-space form:

$$\boldsymbol{\theta}_{k+1} = \boldsymbol{\theta}_k + \boldsymbol{\omega}_k, \tag{7}$$

$$V_{\mathrm{o},k} = g\left(\boldsymbol{x}_k, I_k, \boldsymbol{\theta}_k\right) + \nu_k, \tag{8}$$

where

$$\boldsymbol{x}_k = \begin{bmatrix} S_k & V_{1,k} & V_{2,k} \end{bmatrix}^\mathrm{T}, \tag{9}$$

$$g\left(\boldsymbol{x}_k, I_k, \boldsymbol{\theta}_k\right) = K_0 + K_1 \ln\left(\frac{S_k}{1-S_k}\right) - V_{1,k} - V_{2,k} - I_k^+ R_3^+ - I_k^- R_3^-, \tag{10}$$

where $\boldsymbol{\theta}$ denotes the battery parameter vector and $\boldsymbol{\theta}$=[K_0 K_1 η α_1 b_1 α_2 b_2 R_3^+ R_3^-]$^\mathrm{T}$; V_o is the output voltage of the battery. Different values of the ohmic resistance R_3 are employed for the discharging and charging processes of the battery, R_3^+ and R_3^- correspond to the discharging and charging resistances, respectively; I_k^+ and I_k^- correspond to the discharging and charging currents, respectively. When discharging the battery, $I_k^+ = I_k$ and $I_k^- = 0$; when charging the battery, $I_k^+ = 0$ and $I_k^- = I_k$. $\boldsymbol{\omega}$ is the process noise, which is assumed to be zero-mean and Gaussian white noise. ν is the measurement noise which is assumed to be also zero-mean and Gaussian white noise. The extended Kalman filtering equations for the process depicted by Eqs. (7) and (8) are given below. The decoration "circumflex" is used to represent an estimated quantity.

1. Time update

$$\hat{\boldsymbol{\theta}}_{k|k-1} = \hat{\boldsymbol{\theta}}_{k-1}, \tag{11}$$

$$\boldsymbol{P}_{k|k-1} = \boldsymbol{P}_{k-1} + \boldsymbol{Q}, \tag{12}$$

where $\boldsymbol{P}$ represents the estimation error covariance for $\hat{\boldsymbol{\theta}}$, $\boldsymbol{Q}$ is the covariance of the process noise $\boldsymbol{\omega}$, and the subscript $k|k-1$ is used to denote the time instant before the measurement at time step k is given.

2. Measurement update

$$\boldsymbol{G}_k = \boldsymbol{P}_{k|k-1}\boldsymbol{C}_k^\mathrm{T}\left[\boldsymbol{C}_k \boldsymbol{P}_{k|k-1}\boldsymbol{C}_k^\mathrm{T} + W\right]^{-1}, \tag{13}$$

$$\hat{\boldsymbol{\theta}}_k = \hat{\boldsymbol{\theta}}_{k|k-1} + \boldsymbol{G}_k\left[V_{\mathrm{o},k} - g\left(\hat{\boldsymbol{x}}_k, I_k, \hat{\boldsymbol{\theta}}_{k|k-1}\right)\right], \tag{14}$$

$$\boldsymbol{P}_k = \left(\boldsymbol{E} - \boldsymbol{G}_k \boldsymbol{C}_k\right)\boldsymbol{P}_{k|k-1}, \tag{15}$$

where

$$\boldsymbol{C}_k = \frac{\mathrm{d}g\left(\hat{\boldsymbol{x}}_k, I_k, \boldsymbol{\theta}\right)}{\mathrm{d}\boldsymbol{\theta}}\Big|_{\boldsymbol{\theta}=\hat{\boldsymbol{\theta}}_{k|k-1}}, \tag{16}$$

where W is the covariance of the measurement noise ν, $\boldsymbol{G}$ is the Kalman gain, and $\boldsymbol{E}$ is an identity matrix. Given $\hat{\boldsymbol{\theta}}_{k-1}$ and $\hat{\boldsymbol{x}}_{k-1}$, $\hat{\boldsymbol{x}}_k$ is computed using Eq. (1). After initialization, repeat the foregoing time and measurement update equations, so as to recursively achieve the estimated parameter vector $\hat{\boldsymbol{\theta}}_k$. Although $\hat{\boldsymbol{x}}_k$ is noisy due to the estimation error of $\hat{\boldsymbol{\theta}}_{k-1}$, as the recursion times increase, a good calibration result can be expected. Additionally, since $\hat{\boldsymbol{x}}_k$ is a function of the parameter vector $\boldsymbol{\theta}$, the calculation of $\boldsymbol{C}_k$ involves complicatedly recurrent derivatives, which are shown as follows:

$$\frac{\mathrm{d}g\left(\hat{\boldsymbol{x}}_k, I_k, \boldsymbol{\theta}\right)}{\mathrm{d}\boldsymbol{\theta}} = \frac{\partial g\left(\hat{\boldsymbol{x}}_k, I_k, \boldsymbol{\theta}\right)}{\partial \boldsymbol{\theta}} + \frac{\partial g\left(\hat{\boldsymbol{x}}_k, I_k, \boldsymbol{\theta}\right)}{\partial \hat{\boldsymbol{x}}_k}\frac{\mathrm{d}\hat{\boldsymbol{x}}_k}{\mathrm{d}\boldsymbol{\theta}}, \tag{17}$$

$$\frac{\mathrm{d}\hat{\boldsymbol{x}}_k}{\mathrm{d}\boldsymbol{\theta}} = \frac{\partial \boldsymbol{f}\left(\hat{\boldsymbol{x}}_{k-1}, I_{k-1}, \boldsymbol{\theta}\right)}{\partial \boldsymbol{\theta}} + \frac{\partial \boldsymbol{f}\left(\hat{\boldsymbol{x}}_{k-1}, I_{k-1}, \boldsymbol{\theta}\right)}{\partial \hat{\boldsymbol{x}}_{k-1}}\frac{\mathrm{d}\hat{\boldsymbol{x}}_{k-1}}{\mathrm{d}\boldsymbol{\theta}}, \tag{18}$$

where

$$\frac{\partial g(\hat{\boldsymbol{x}}_k, I_k, \boldsymbol{\theta})}{\partial \boldsymbol{\theta}} = \left[1 \quad \ln\left(\frac{\hat{S}_k}{1-\hat{S}_k}\right) \quad 0 \quad 0 \quad 0 \quad 0 \quad 0 \quad -I_k^+ \quad -I_k^- \right], \tag{19}$$

$$\frac{\partial g(\hat{\boldsymbol{x}}_k, I_k, \boldsymbol{\theta})}{\partial \hat{\boldsymbol{x}}_k} = \left[\frac{\hat{K}_{1,k-1}}{\hat{S}_k\left(1-\hat{S}_k\right)} \quad -1 \quad -1 \right], \tag{20}$$

$$\frac{\partial \boldsymbol{f}(\hat{\boldsymbol{x}}_{k-1}, I_{k-1}, \boldsymbol{\theta})}{\partial \boldsymbol{\theta}} = \begin{bmatrix} 0 & 0 & \frac{-\Delta t}{C_n} & 0 & 0 & 0 & 0 & 0 & 0 \\ 0 & 0 & 0 & \hat{V}_{1,k-1} & I_{k-1} & 0 & 0 & 0 & 0 \\ 0 & 0 & 0 & 0 & 0 & \hat{V}_{2,k-1} & I_{k-1} & 0 & 0 \end{bmatrix}, \tag{21}$$

$$\frac{\partial \boldsymbol{f}(\hat{\boldsymbol{x}}_{k-1}, I_{k-1}, \boldsymbol{\theta})}{\partial \hat{\boldsymbol{x}}_{k-1}} = \begin{bmatrix} 1 & 0 & 0 \\ 0 & \hat{\alpha}_{1,k-1} & 0 \\ 0 & 0 & \hat{\alpha}_{2,k-1} \end{bmatrix}. \tag{22}$$

It is clear that the derivative calculations are recursive. The calculation of recurrent derivatives can be initialized as follows:

$$\frac{\mathrm{d}\hat{\boldsymbol{x}}_0}{\mathrm{d}\boldsymbol{\theta}} = 0. \tag{23}$$

4 Results and discussion

Two different transient power tests for an EV lithium iron phosphate battery were conducted to validate the calibration algorithm. One was the Federal Urban Driving Schedule (FUDS) test, the other was a variant of the standard Dynamic Stress Test (DST). The two transient power-based tests can be used to simulate the actual loading conditions of the battery in daily driving of EVs. Since the battery SOC is rarely allowed to be below 10% in actual EV applications, the data sampled in the SOC range from 98% to 10% was only applied to evaluate the calibration algorithm. The lithium iron phosphate battery had a nominal voltage of 3.2 V, a nominal capacity of 12 Ah, and an initial SOC of 98% in the two tests.

The current and voltage of the battery in the FUDS test are shown in Fig. 2. According to *a priori* knowledge on the battery system, the parameters for the extended Kalman filtering calibration algorithm are specified as follows:

$$\hat{\boldsymbol{x}}_0 = [98\% \quad 0 \quad 0]^{\mathrm{T}}, \tag{24}$$

$$\hat{\boldsymbol{\theta}}_0 = \left[3 \quad 0.02 \quad 0.98 \quad \mathrm{e}^{-1/3} \quad \frac{1-\mathrm{e}^{-1/3}}{100} \quad \mathrm{e}^{-1/10} \quad \frac{1-\mathrm{e}^{-1/10}}{100} \quad 0.01 \quad 0.01 \right]^{\mathrm{T}}, \tag{25}$$

$$\boldsymbol{Q} = \mathrm{diag}\{[0 \quad 0 \quad 0 \quad 5\times10^{-8} \quad 5\times10^{-8} \quad 10^{-8} \quad 10^{-8} \quad 3\times10^{-8} \quad 3\times10^{-8}]^{\mathrm{T}}\}, \tag{26}$$

$$W = 0.5, \tag{27}$$

$$\boldsymbol{P}_0 = \mathrm{diag}\{[0.25 \quad 10^{-4} \quad 9\times10^{-4} \quad 0.25 \quad 10^{-4} \quad 0.25 \quad 10^{-4} \quad 10^{-4} \quad 10^{-4}]^{\mathrm{T}}\}, \tag{28}$$

where diag{[⋯]} denotes a diagonal matrix in which [⋯] is on the main diagonal.

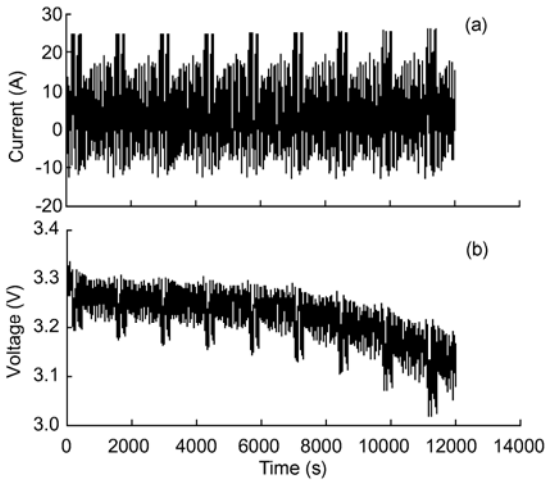

Fig. 2 Current (a) and voltage (b) profiles in the FUDS test

Given the current, voltage and parameters shown in Eqs. (24)–(28), the extended Kalman filtering-based calibration algorithm can be implemented. The results of the calibrated parameters are shown in Figs. 3–5. Trajectories of $\hat{K}_0$ and $\hat{K}_1$ are shown in Fig. 3. It can be seen that $\hat{K}_0$ is convergent after quickly correcting the initial error and $\hat{K}_1$ has a slow time-varying characteristic. Results of $\hat{\alpha}_1$, $\hat{b}_1$, $\hat{\alpha}_2$

and $\hat{b}_2$ in the calibration process are shown in Fig. 4. It can be seen that $\hat{\alpha}_2$ is larger than $\hat{\alpha}_1$. This result indicates that the time constant of the R_2C_2 network is larger than that of the R_1C_1 network. Additionally, a rising trend can be seen for both $\hat{\alpha}_1$ and $\hat{\alpha}_2$, due to a falling trend of the battery SOC in the FUDS test. Trajectories of $\hat{\eta}$, $\hat{R}_3^+$ and $\hat{R}_3^-$ are shown in Fig. 5. It can be observed that the estimated Coulombic efficiency $\hat{\eta}$ has a relatively small change. It also can be observed that the estimated discharging resistance $\hat{R}_3^+$ has smaller values at middle (70%–50%) SOC values in comparison with those at high (98%–90%) and low (20%–10%) SOC values. The estimated charging resistance $\hat{R}_3^-$ has relatively stable values, since the discharging process is dominant in a standard FUDS cycle.

The simulated and measured battery voltages are shown in Fig. 6. A magnified part is also shown to give more details. It is obvious that the calibrated battery model can accurately describe the voltage behavior of the lithium iron phosphate battery after correcting the initial error of the model parameter vector. In order to better evaluate the battery model, the relative voltage error is shown in Fig. 7. The maximum error can quickly converge to be less than 1%, indicating an effectiveness of the recursive calibration algorithm. The mean relative error is 0.204%.

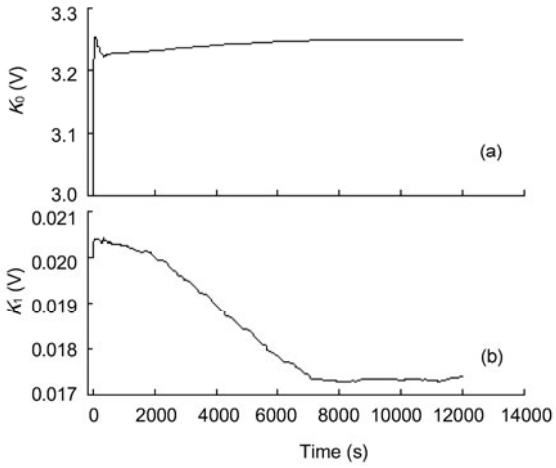

Fig. 3 Trajectories of $\hat{K}_0$ (a) and $\hat{K}_1$ (b) in the calibration process

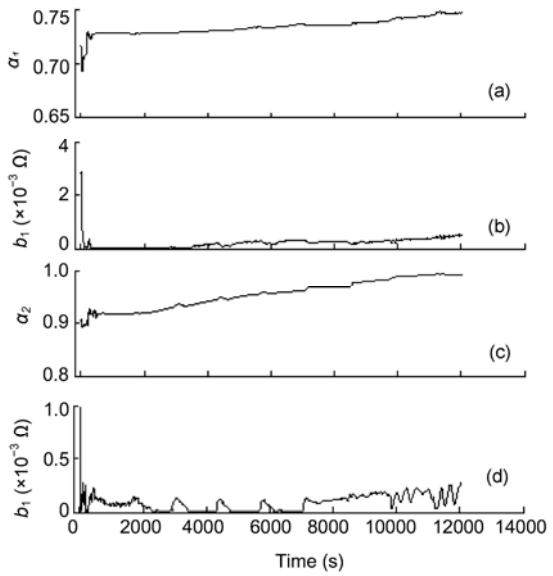

Fig. 4 Trajectories of $\hat{\alpha}_1$ (a), $\hat{b}_1$ (b), $\hat{\alpha}_2$ (c) and $\hat{b}_2$ (d) in the calibration process

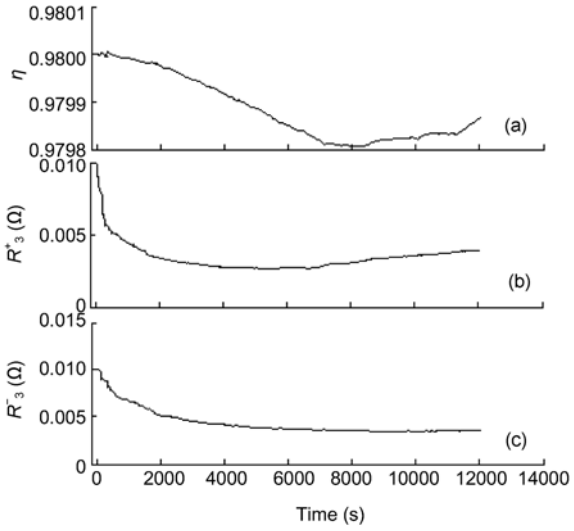

Fig. 5 Trajectories of $\hat{\eta}$ (a), R_3^+ (b) and R_3^- (c) in the calibration process

For the modified DST test, the current and voltage of the battery are shown in Fig. 8. The parameters for the calibration algorithm were the same as those used in the FUDS test. For simplicity, the estimated trajectories of the model parameters are not illustrated here. The simulated and measured battery voltage responses are shown in Fig. 9, in which a magnified view is also provided. It is clear that the recursively calibrated model can precisely capture the actual voltage response after compensating

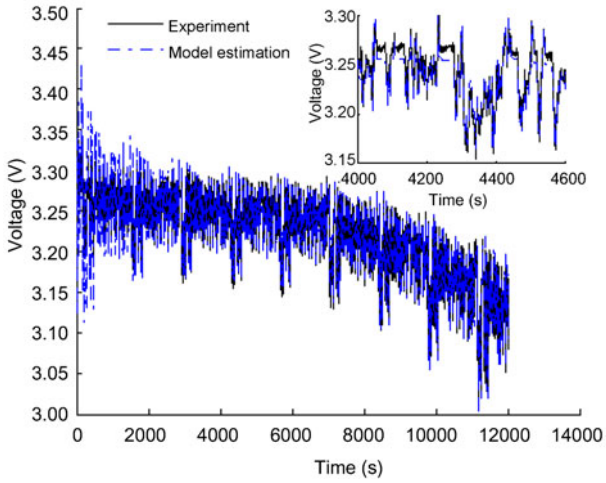

Fig. 6 Simulated and measured battery voltages in the FUDS test

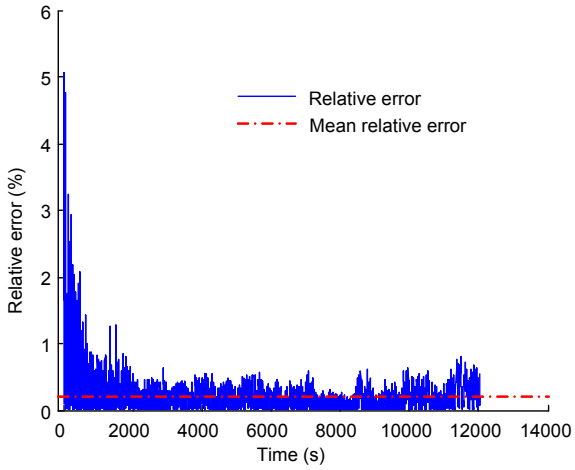

Fig. 7 Relative error of the model in the FUDS test

for the initial model error. The relative voltage error in the modified DST test is shown in Fig. 10 to more straightforwardly demonstrate the performance of the model. The mean relative error is 0.369%.

A comparison with a first-order model was also made. The first-order model (Hu *et al*., 2011) was obtained by removing one parallel resistance-capacitance network from the proposed model. In order to ensure a fair comparison, extended Kalman filtering was also used to identify the first-order model. The comparison results are shown in Fig. 11 and Fig. 12. Herein, the relative voltage errors for the two models are presented instead of the estimated voltage responses. Therefore, the performance difference between the two models can be more

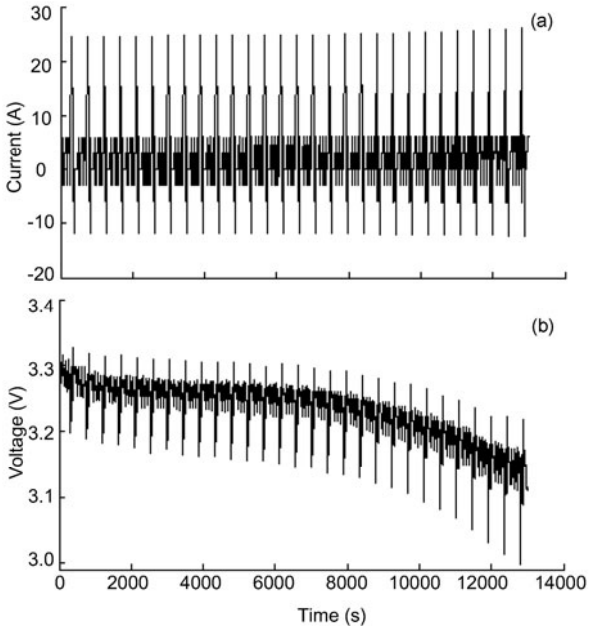

Fig. 8 Current (a) and voltage (b) profiles in the modified DST test

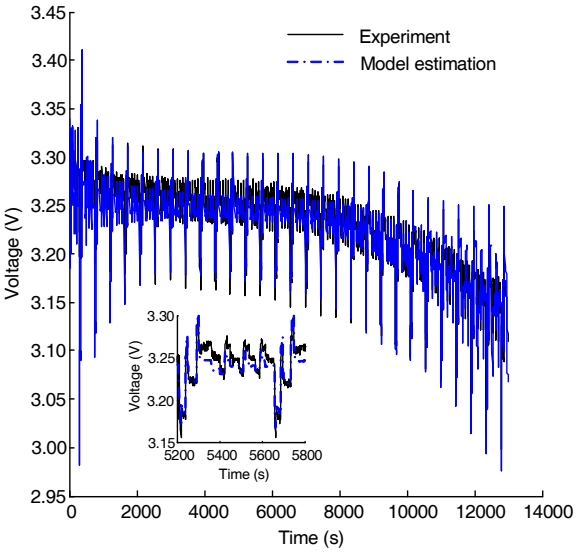

Fig. 9 Simulated and measured battery voltages in the modified DST test

conveniently observed. After correcting the initial errors, the two battery models had comparable accuracies in a considerable part of the battery SOC range. After around 9000 s in the two tests, the first-order model presented larger estimation errors than did the second-order model. The accuracy deviation may be caused by a serious polarization effect of the battery

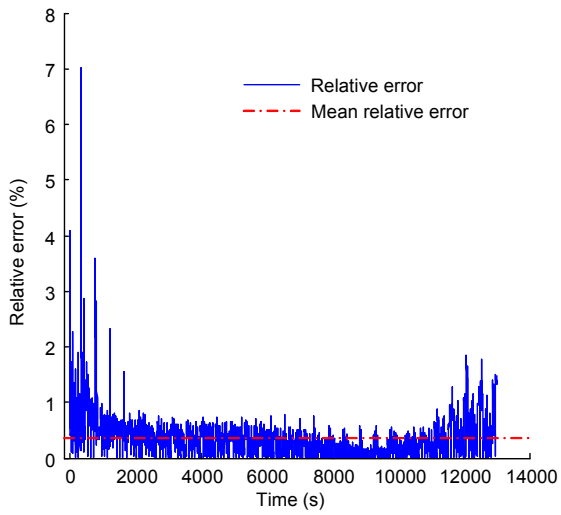

Fig. 10 Relative error of the model in the modified DST test

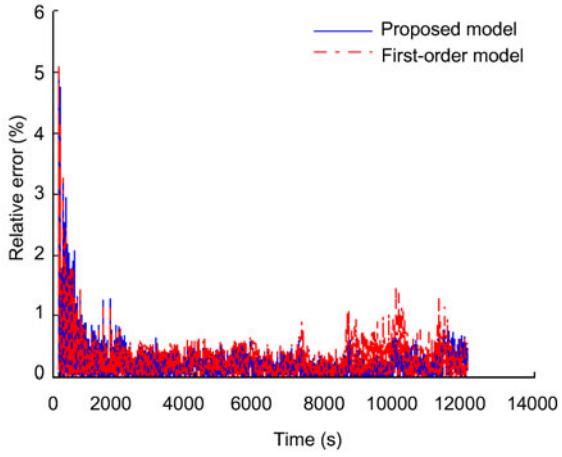

Fig. 11 Comparison result in the FUDS test

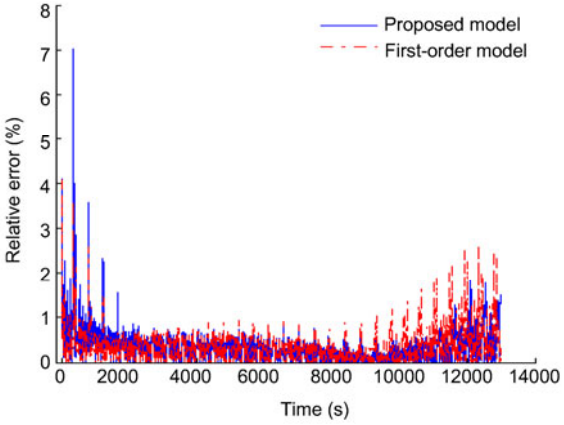

Fig. 12 Comparison result in the modified DST test

with a relatively low capacity. The two resistance-capacitance networks could be more effective to depict large overpotentials generated by the serious polarization. Despite a better accuracy at low SOC values, the second-order model has a more complicated structure, which results in a heavier computational load. Thus, it is reasonable to depend on actually predominant requirements for on-board battery management applications to determine which model is more suitable. For example, if operating the battery at relatively low SOC values (e.g., 20%–10%) in actual electric vehicle operations is allowed and the computational cost is not a main concern, the second-order battery model recursively identified by extended Kalman filtering will be better.

5 Conclusions

1. A model structure that consists of a second-order resistance-capacitance network and a simply analytical OCV-SOC map is proposed to characterize the voltage behavior of an EV lithium iron phosphate battery. As a result, the model parameterization can be readily realized.

2. Extended Kalman filtering is applied to recursively calibrate the battery model. The linearization involved in extended Kalman filtering was implemented through recurrent derivatives in a recursive form.

3. Validation results show that the recursively calibrated battery model can accurately depict the battery voltage behavior under two different battery operating situations. The recursive calibration algorithm can guarantee that the battery model has good robustness against varying battery loading profiles.

4. A comparison with a first-order model indicates that the recursively identified second-order model has a comparable accuracy in a large portion of the battery SOC range and a better performance when the SOC is relatively low (<20%).

5. Future work could focus on simultaneous SOC and SOH estimation based on the recursively calibrated model. Model update and SOC estimation could be coupled to investigate battery monitoring and control in the long-time aging process of the battery.

References

Dai, H.F., Sun, Z.C., Wei, X.Z., 2009. Estimation of internal states of power lithium-ion batteries used on electric vehicles by dual extended Kalman filter. *Journal of Mechanical Engineering*, **45**(6):95-101 (in Chinese).

Han, J.Y., Kim, D.C., Sunwoo, M., 2009. State-of-charge estimation of lead-acid batteries using an adaptive extended Kalman filter. *Journal of Power Sources*, **188**(2): 606-612.

Hu, X.S., Sun, F.C., Zou, Y., 2010a. Estimation of state of charge of a lithium-ion battery pack for electric vehicles using an adaptive Luenberger observer. *Energies*, **3**(9):1586-1603. [doi:10.3390/en3091586]

Hu, X.S., Sun, F.C., Cheng, X.M., 2010b. Fuzzy model for estimation of the state-of-charge of lithium-ion batteries for electric vehicles. *Journal of Beijing Institute of Technology*, **19**(4):416-421.

Hu, X.S., Sun, F.C., Zou, Y., 2011. Online model identification of lithium-ion battery for electric vehicles. *Journal of Central South University of Technology*, **18**(5): 1525-1531. [doi: 10.1007/s11771-011-0869-1]

Kim, I.S., 2006. The novel state of charge estimation method for lithium battery using sliding mode observer. *Journal of Power Sources*, **163**(1):584-590. [doi:10.1016/j.jpowsour.2006.09.006]

Kim, I.S., 2008. Nonlinear state of charge estimator for hybrid electric vehicle battery. *IEEE Transactions on Power Electronics*, **23**(4):2027-2034. [doi:10.1109/TPEL.L2008.924629]

Li, C., 2007. Research on Model Identification and SOC Estimation for EV NiMH Battery. MS Thesis, Tianjin University, Tianjin, China (in Chinese).

Lin, C.T., Qiu, B., Chen, Q.S., 2005. Comparison of current input equivalent circuit models of electric vehicle battery. *Chinese Journal of Mechanical Engineering*, **41**(12): 76-81.

Lin, X., Pan, S.X., Wang, D.Y., 2008. Dynamic simulation and optimal control strategy for a parallel hybrid hydraulic excavator. *Journal of Zhejiang University SCIENCE-A*, **9**(5):624-632. [doi:10.1631/jzus.A071552]

Ota, Y., Sakamoto, M., Kiriake, R., Kobe, T., Hashimoto, Y., 2008. Modeling of Voltage Hysteresis and Relaxation of HEV NiMH Battery. The 17th IFAC World Congress, Seoul, Korea. IFAC, New York, USA, p.4654-4658. [doi:10.3182/20080706-5-KR-1001.00783]

Plett, G.L., 2004. Extended Kalman filtering for battery management systems of LiPB-based HEV battery packs: Part 2. Modeling and identification. *Journal of Power Sources*, **134**(2):262-276. [doi:10.1016/j.jpowsour.2004.02.032]

Qiang, J.X., Ao, G.Q., Yang, L., 2008. Estimation method on the battery state of charge for hybrid electric vehicle. *Chinese Journal of Mechanical Engineering*, **21**(3): 20-25.

Sciarretta, A., Back, M., Guzzella, L., 2004. Optimal control of parallel hybrid electric vehicles. *IEEE Transactions on Control System Technology*, **12**(3):352-363. [doi:10.1109/TCST.2004.824312]

Sun, F.C., Hu, X.S., Zou, Y., Li, S.G., 2011. Adaptive unscented Kalman filtering for state of charge estimation of a lithium-ion battery for electric vehicles. *Energy*, **36**(5):3531-3540. [doi:10.1016/j.energy.2011.03.059]

Verbrugge, M., 2007. Adaptive, multi-parameter battery state estimator with optimized time-weighting factors. *Journal of Applied Electrochemistry*, **37**(5):605-616. [doi:10.1007/s10800-007-9291-7]

Wang, J.P., Cao, B.G., Chen, Q.S., Wang, F., 2007. Combined state of charge estimator for electric vehicle battery pack. *Control Engineering Practice*, **15**(12):1569-1576. [doi:10.1016/j.conengprac.2007.03.004]

Xiong, W.W., Zhang, Y., Yin, C.L., 2009. Configuration design, energy management and experimental validation of a novel series-parallel hybrid electric transit bus. *Journal of Zhejiang University SCIENCE-A*, **10**(9):1269-1276. [doi:10.1631/jzus.A0820556]

2010 JCR of Thomson Reuters for *JZUS-A* and *JZUS-B*

ISI Web of Knowledge℠

Journal Citation Reports®

WELCOME | HELP | RETURN TO LIST

2010 JCR Science Edition

Journal: Journal of Zhejiang University-SCIENCE A

Mark	Journal Title	ISSN	Total Cites	Impact Factor	5-Year Impact Factor	Immediacy Index	Citable Items	Cited Half-life	Citing Half-life
☐	J ZHEJIANG UNIV-SC A	1673-565X	442	0.322		0.050	120	3.7	7.1

Journal: Journal of Zhejiang University-SCIENCE B

Mark	Journal Title	ISSN	Total Cites	Impact Factor	5-Year Impact Factor	Immediacy Index	Citable Items	Cited Half-life	Citing Half-life
☐	J ZHEJIANG UNIV-SC B	1673-1581	770	1.027		0.137	124	3.5	7.5